

Photochemistry

Distance Matters: Effect of the Spacer Length on the Photophysical Properties of Multimodular Perylenediimide-Silicon Phthalocyanine-Fullerene Triads

Luis Martín-Gomis, [a] Rocío Díaz-Puertas, [a] Sairaman Seetharaman, [b] Paul A. Karr, [c] Fernando Fernández-Lázaro, [a] Francis D'Souza, *[b] and Ángela Sastre-Santos *[a]

Dedicate to Professor Atsuhiro Osuka on the occasion of his 65th birthday

Abstract: A multimodular donor–acceptor conjugate featuring silicon phthalocyanine (SiPc) as the electron donor, and two electron acceptors, namely tetrachloroperylenediimide (PDI) and C_{60} , placed at the opposite ends of the SiPc axial positions, was newly designed and synthesized, and the results were compared to the earlier reported PDI-SiPc- C_{60} triad. Minimal intramolecular interactions between the entities was observed. Absorption, fluorescence, computational and electrochemical studies were performed to evaluate the excitation energy, geometry and electronic structure, and energy levels of different photoevents. Steady-state absorp-

tion, fluorescence and excitation spectral studies revealed efficient singlet–singlet energy transfer from $^1\text{PDI*}$ to SiPc in the PDI-SiPc dyad and the PDI-SiPc- C_{60} triad. The measured rates for these photochemical events were found to be much higher than those reported earlier for the triad, due to closer proximity between the PDI and SiPc entities. The distance also affected the charge separation path in which involvement of PDI, and not C_{60} , in charge separation in the present triad was witnessed. The present investigation brings out the importance of donor–acceptor distances in channeling photochemical events in a multimodular system.

Introduction

Taking advantage of the vast amount of sunlight, and transforming it into electric power is, probably, one of the most investigated topics in recent years. Humanity is slowly becoming aware of the real necessity to stop consuming fossil fuels, and utilize clean and renewable energy. In this context, mimicking the natural photosynthesis process appears to be a simple, yet effective, strategy to get molecular systems that are able to absorb and convert light to chemical or electrical energy. From the point of view of molecular design, the combination of electron donor and electron acceptor subunits, with at least one of them playing the antenna role, is the most

straightforward strategy to obtain artificial photosynthetic systems. These systems absorb light and trigger a sequence of consecutive cascade of energy and/or electron processes, to finally afford a long-lived charged separated state, potentially useful in photovoltaic and photocatalytic applications. [9,10] There are a variety of chemically stable building blocks, easy to synthesize and functionalize and, therefore, with tunable light harvesting and photophysical properties, suitable to "construct" high-performance artificial photosynthetic systems. Among the available building blocks, perylenediimides (PDI), $^{[11-13]}$ phthalocyanines (Pcs) $^{[14-16]}$ and C_{60} -fullerene $^{[17,18]}$ stand up. PDI and Pcs exhibit large molar extinction coefficients, up to $10^5 \,\mathrm{m}^{-1} \,\mathrm{cm}^{-1}$, with absorption and emission spectra covering the 400-800 nm region. They also present genuine electron-acceptor and electron-donor characters, respectively, which can be modulated through chemical modifications. On the other hand, C₆₀-fullerene is a well-known electron-acceptor moiety, due to its large π -electron 3D spherical system, which makes it to present a small reorganization energy after reduction, which results in fast charge separation process and slow recombination of the formed charged separated state. It is easy to infer that combinations of these three building blocks would potentially fulfill the necessary requirements for highly efficient artificial photosynthetic systems, absorbing most of the solar spectrum, and rapidly transferring to afford long-lived charged separated states. Synthesis of covalent and supramolecular ensembles of PDI, Pc and C₆₀ have been described within recent scientific literature, and their

[a] Dr. L. Martín-Gomis, R. Díaz-Puertas, Prof. Dr. F. Fernández-Lázaro, Prof. Dr. Á. Sastre-Santos División de Química Orgánica, Instituto de Bioingeniería Universidad Miguel Hernández, Avda. de la Universidad s/n 03203 Elche (Spain) E-mail: asastre@umh.es

[b] S. Seetharaman, Prof. Dr. F. D'Souza Department of Chemistry, University of North Texas at Denton 1155 Union Circle, #305070, Denton, TX 76203-5017 (USA) E-mail: Francis.DSouza@unt.edu

[c] Prof. Dr. P. A. Karr Department of Physical Sciences and Mathematics Wayne State College, 1111 Main Street, Wayne, Nebraska, 68787 (USA)

Supporting information and the ORCID identification number(s) for the author(s) of this article can be found under: https://doi.org/10.1002/chem.201905605.

Wiley Online Library



photophysical properties have been also studied. [4–8] In this context, our groups have recently published the synthesis of a multichromophoric PDI-SiPc- C_{60} covalent system (compound **10** in Figure 1) and its photophysical characterization after selective irradiation of either PDI or SiPc chromophores. [19] It was concluded that, upon selective irradiation of the PDI moiety, a sequence of energy transfer to SiPc, followed by electron transfer to PDI or/and C_{60} occurs, being the fullerene moiety the most involved unit in the final electron transfer reaction, even though PDI is, in this case, a better electron acceptor. This was attributed to the geometrical arrangement of

electron acceptors around central SiPc core, where C_{60} is much closer than PDI. To rationalize this hypothesis, here we describe the synthesis, characterization, and photophysical properties of a new triad, PDI-SiPc- C_{60} 1 (see Figure 1), specially designed to bear electroactive subunits, PDI and C_{60} , rigidly connected through a p-phenylbenzoate linker, in the axial positions of a silicon phthalocyanine (SiPc), thus affording a multichromophoric triad where electron acceptor units are equidistant to central SiPc core.

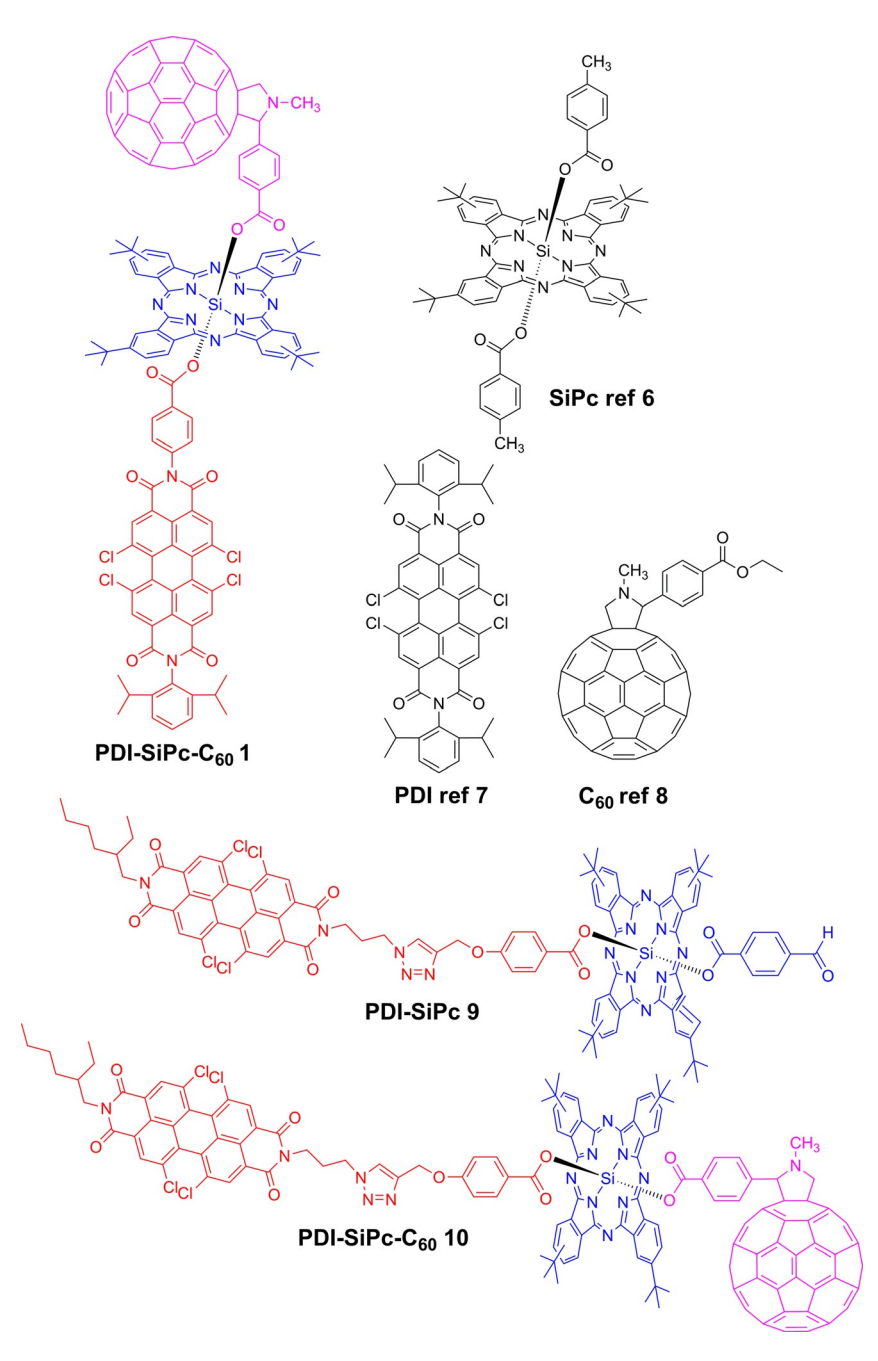


Figure 1. Chemical structure of the newly synthesized PDI-SiPc- C_{60} 1 and the control compounds. Structure of the earlier reported dyad 9 and triad 10 with flexible linker is also shown for comparison purposes.

www.chemeurj.org

Scheme 1. Synthesis of PDI-SiPc dyad 3 and PDI-SiPc-C₆₀ triad 1.

Results and Discussion

Synthesis

The synthesis of PDI-SiPc- C_{60} triad 1 is described in Scheme 1. Equimolar quantities of p-formylbenzoic acid and PDI 2 react with tetra-tert-butyl silicon phthalocyanine dichloride to obtain the asymmetrically axial-substituted phthalocyanine PDI-SiPc-CHO 3 in a 6% yield. That statistical condensation is the bottleneck of the synthetic strategy employed, but taking into account the molar ratio, reaction time and the unavoidable obtention of symmetrically axial-substituted phthalocyanine compounds (PDI) $_2$ SiPc and SiPc(CHO) $_2$, a 6% yield perfectly agrees to those we have already obtained, employing comparable experimental conditions, in the synthesis of similar compounds. Finally, PDI-SiPc-CHO 3 was reacted with C_{60} fullerene and N-methylglycine, through an 1,3-dipolar cycloaddition of in situ generated azomethine ylide C_{60} to afford PDI-SiPc-CG0 triad 1 in 75% yield.

All of the new compounds were fully characterized with standard techniques. Figure 2 shows a well-resolved ¹H NMR spectrum of PDI-SiPc-C₆₀ triad 1, recorded in deuterated chloroform, in which characteristic signals can be assigned (see also Figure S1, Supporting Information, for ¹H NMR of **2**). For example, the aromatic hydrogen atoms of the phthalocyanine ring appear as two multiplets, at 9.85-9.55 and 8.45 ppm, integrating for eight and four hydrogen atoms, respectively, while ortho hydrogens of asymmetric tetrachloro-perylendiimide moiety appear as two sharp singlets, centered at 8.67 and 8.39 ppm integrating for two hydrogen atoms each. The Nmethylfulleropyrrolidine hydrogen signals look like two coupled doublets and a singlet in between, centered at 4.63, 3.87 and 4.28 ppm, respectively; furthermore, one singlet integrating for three hydrogens is centered at 2.20 ppm. At this point, it is worth noting that aromatic hydrogens of benzoate linkers appear in the middle part of the spectrum, because the influ-

www.chemeurj.org

ence of the strong ring current of the phthalocyanine. Concretely, two sets of coupled signals can be distinguished, at 6.70 and 5.26 ppm, those corresponding to p-phenyl fulleropyrrolidine union, whereas other two doublets, centered at 6.19 and 5.35 ppm, are assigned to the analog axial connection with perylenediimide subunit. On the other hand, the mass spectrum of the PDI-SiPc- C_{60} triad 1 shows a very low intense molecular ion peak at m/z 2469.511 amu ($[M+H]^+$), with an isotopic distribution that exactly matches the simulated isotopic pattern, and two intense signals at m/z 1572.300 and 1662.363 amu, which correspond to the loss of the axial substituents, N-methylfulleropyrrolidinebenzoate and tetrachloroperylene diimide benzoate, respectively (see Figures S2 and S3 for dyad and triad mass spectrum, Supporting Information).

Optical absorption fluorescence and electrochemical studies

Systematic absorption and fluorescence studies were performed to probe ground- and excited-state interactions in the PDI-SiPc dyad **3** and in the PDI-SiPc-C₆₀ triad **1** in benzonitrile. As shown in Figure 3 a, a comparison between the absorption spectra of the dyad and triad were a simple addition of their individual components, suggesting minimal ground state interactions between the entities, that is, no noticeable spectral shift or broadening was observed. In these spectra, PDI absorption in the 450–550 nm range, and SiPc absorption in the 600–740 nm range are noteworthy. The isolated absorption peaks provide an opportunity to selectively excite the PDI and SiPc entities in the dyad and triad.

The PDI fluorescence was characterized by a broad peak at 550 nm covering the spectral ranges of 440–680 nm, whereas that of SiPc has a peak maximum at 705 nm with spectral coverage spanning 675–760 nm range. When the fluorescence spectrum of equimolar PDI and SiPc was recorded at the excitation wavelength of 492 nm corresponding to PDI excitation,

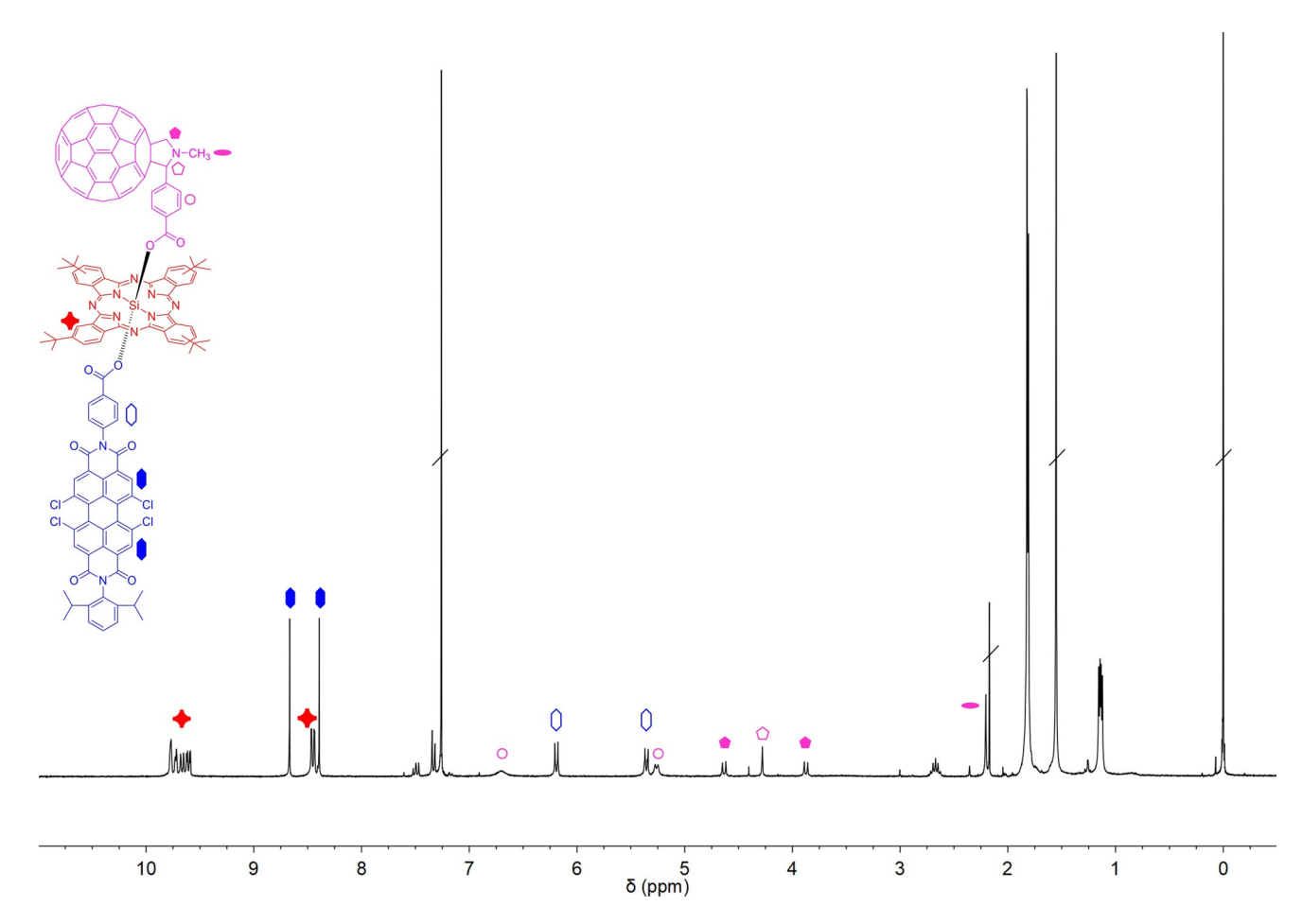


Figure 2. ^{1}H NMR spectrum of PDI-SiPc-C $_{60}$ triad 1 in CDCI $_{3}$.

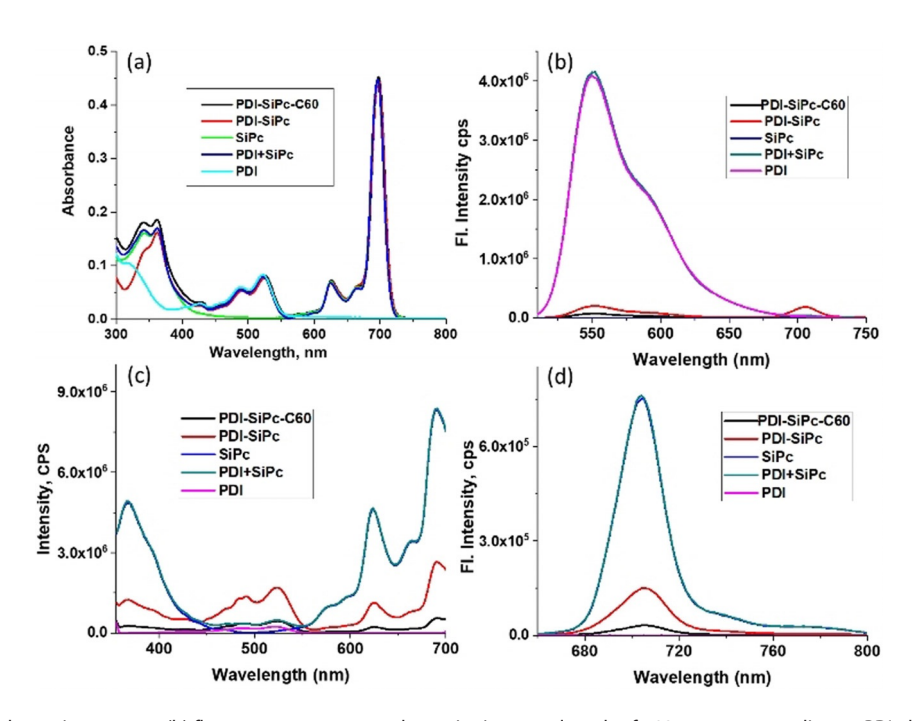


Figure 3. (a) Normalized absorption spectra, (b) fluorescence spectra at the excitation wavelength of 492 nm corresponding to PDI absorption, (c) excitation spectra recorded by holding the emission monochromator to 705 nm, corresponding to SiPc emission, while scanning the excitation wavelength, and (d) fluorescence spectra at the excitation wavelength of 625 nm, corresponding to SiPc absorption. All spectra were recorded in benzonitrile.

no appreciable quenching of PDI emission or appearance of SiPc fluorescence was observed, suggesting the absence of intermolecular-type interactions between them (Figure 3b). Interestingly, in the case of PDI-SiPc dyad 3, upon selective excitation of PDI, quenching of PDI over 95% was observed with the appearance of SiPc emission around 706 nm. For the triad, additional quenching of both PDI and SiPc emission was witnessed (98% quenching of PDI fluorescence). These results suggest the occurrence of singlet-singlet energy transfer in the dyad, resulting in ¹SiPc* as energy transfer product.^[27] Additional evidence for energy transfer came from recording the excitation spectrum of the dyad, wherein the emission monochromator was fixed to SiPc emission maxima while scanning wavelength of the excitation monochromator. Such spectra, for the investigated compounds along with the control compounds, are shown in Figure 3 c. For PDI-SiPc dyad 3, as expected, peaks corresponding to both PDI and SiPc were clearly observed providing direct proof for the occurrence of energy transfer. In the case of PDI-SiPc-C₆₀ triad 1 with an additional fullerene electron acceptor, excitation peaks corresponding to both PDI and SiPc revealed diminished intensities.

Changing the excitation wavelength to 625 nm, corresponding to SiPc excitation, revealed additional interesting observations (Figure 3 d). That is, quenching of SiPc emission in the amount of 80% in the case of the dyad and 95% in the case of triad was observed. However, no quenching of SiPc in a 1:1 mixture of PDI and SiPc was observed indicating involvement of ¹SiPc* in additional photochemical events in the covalently linked systems.

Next, cyclic voltammetry experiments of PDI-SiPc- C_{60} triad 1 were recorded in benzonitrile, and compared to those of reference compounds SiPc ref. 6, PDI ref. 7 and C_{60} ref. 8 (see Figure 1). Figure 4 and electrochemical data, listed in Table 1, show the reversibility of all processes within the timescale of cyclic voltammetry, with oxidation–reduction potentials, which are comparatively assigned to electroactive units, and perfectly

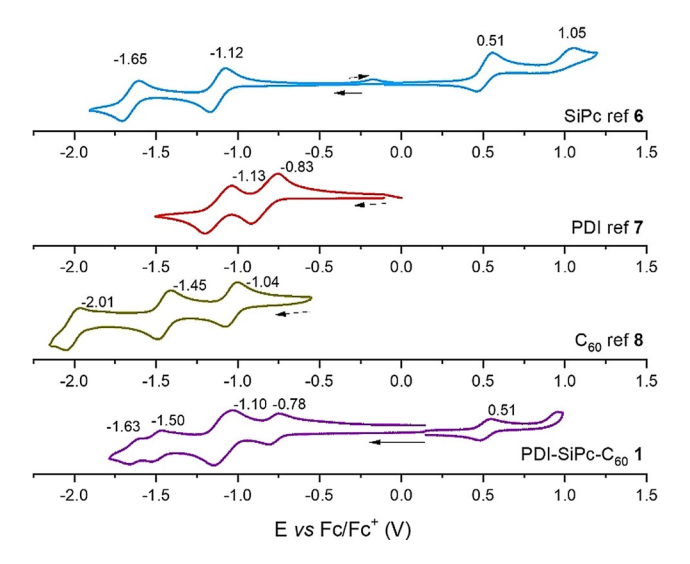


Figure 4. Cyclic voltammograms in PhCN containing Bu_4NPF_6 (0.10 M) of (from top to bottom) SiPc ref. **6**, PDI ref. **7**, C_{60} ref. **8**, and PDI-SiPc- C_{60} **1**. Scan rate: 0.1 V s⁻¹.

www.chemeuri.org

Table 1. Redox potentials $^{[a]}$ of PDI-SiPc-C $_{60}$ 1 and reference compounds SiPc ref. 6, PDI ref. 7 and C $_{60}$ ref. 8 in benzonitrile.

Compound	$E_{\rm red}^{-5}$	$E_{\rm red}^{-4}$	$E_{\rm red}^{-3}$	$E_{\rm red}^{2}$	$E_{\rm red}^{-1}$	$E_{\rm ox}^{-1}$	$E_{\rm ox}^{2}$
1	-	-1.63	-1.50	-1.10 ^[b]	-0.78	0.51	-
6	-	-1.65	-	-1.12	-	0.51	1.05
7	-	-	-	-1.13	-0.83	-	-
8	-2.01	-	-1.45	-1.04	-	-	-

[a] The half-wave potentials measured in volts (vs. Fc/Fc $^+$) are extracted from cyclic voltammograms of solutions in PhCN containing Bu $_4$ NPF $_6$ (0.10 M) as the supporting electrolyte. [b] Overlap of the first reductions of C $_{60}$ and SiPc.

match those obtained for reference compounds. Thus, it could be inferred that the electronic interaction between electron-donor and electron-acceptor units in PDI-SiPc- C_{60} triad 1 is very weak in the ground state, as was also evidenced by spectral studies. As previously reported, the PDI unit bearing four chloro substituents is easier to reduce by nearly 260 mV compared to C_{60} moiety. Based on this, we expected to see primarily an electron transfer from SiPc to PDI over fullerene.

Computational studies and energy level diagram

The geometry and electronic structures of the dyad were deduced from B3LYP/6-311G(d,p) calculations using Gaussian 16 software^[28] and the frontier orbitals were visualized using GaussView software. [29] The structures were fully optimized on Born-Oppenheimer potential energy surface. Figure 5 shows the optimized structure and the frontier HOMO, LUMO and LUMO+1 orbitals of the triad. In the optimized structure, the center-to-center distance between PDI-SiPc and SiPc-C60 were 13.8 Å and 11.6 Å, respectively, whereas the corresponding edge-to-edge distances (from Si to N of PDI and Si to edge of C₆₀) were 8.2 Å and 9.0 Å, respectively. In the recently reported PDI-SiPc-C₆₀ triad, **10**, PDI was held by a flexible linker, ^[19] the edge-to-edge distance between PDI-SiPc was 13.3 Å, much larger compared to that in the present system. Such a close proximity and better electron acceptor ability of PDI might dominate the electron transfer from ¹SiPc* to PDI, leading to

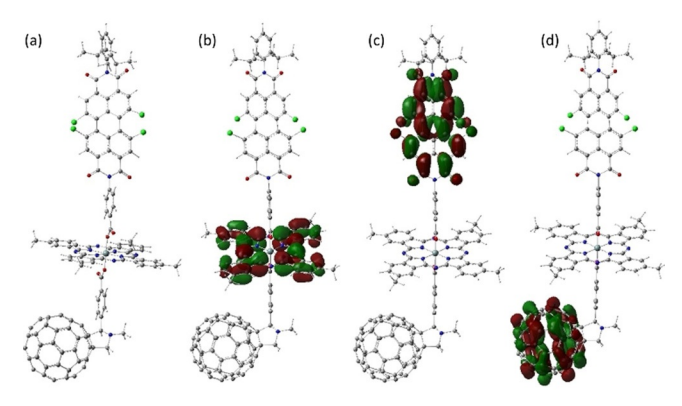


Figure 5. (a) B3LYP/6–311G(d,p) optimized structure, (b) HOMO, (c) LUMO and (d) LUMO $+\,1$ of PDI-SiPc-C $_{60}$ 1 triad.



PDI*-SiPc*+- C_{60} charge separated state instead of PDI-SiPc*+- C_{60} *-

The frontier orbitals also supported better electron acceptor nature of PDI over that of C_{60} in the triad. That is, the LUMO on PDI, LUMO+1 on C_{60} and HOMO on SiPc were witnessed. These results establish the role of PDI being the primary electron acceptor and SiPc being the primary electron donor in the triad.

Energy level diagrams^[30,31] were established to visualize different photochemical events in the dyad (see Figure S4, Supporting Information) and triad (Figure 6). The ¹PDI* formed by selective excitation of PDI in the PDI-SiPc dyad and PDI-SiPc-C₆₀ triad could undergo, thermodynamically feasible singletsinglet energy transfer to generate PDI-1SiPc* in the case of dyad and PDI-1SiPc*-C₆₀ in the case of the triad. Alternatively, a direct electron transfer leading to PDI*--SiPc*+ charge separated state in the case of the dyad and PDI*--SiPc*+-C₆₀ charge separated state in the case of the triad are also thermodynamically feasible. Evidence for the occurrence of singlet-singlet energy transfer has been arrived from the earlier discussed excitation and emission studies. The ¹SiPc* formed either by direct excitation or formed as a product of energy transfer, in the case of the dyad and triad, could undergo electron transfer process to result in PDI*--SiPc*+ charge separated state in the case of the dyad. Interestingly, for the triad there are at least two electron transfer routes involving PDI and C₆₀ electron acceptor entities. Involvement of PDI would generate PDI*--SiPc*+ -C₆₀ charge separated state with radical ion-pair energy of 1.30 eV, whereas C₆₀ involvement would result in PDI-SiPc*+ -C₆₀* charge separated state with an energy of 1.55 eV. Both charge separated state possess energy higher than the energy of triplet states of ³SiPc* (1.26 eV) and ³PDI* (1.07 eV). Under such conditions, the charge separated state would populate one of these triplet excited states, which would eventually relax back to the ground state. In order to probe such mechanistic aspects, pump-probe spectroscopic measurements span-

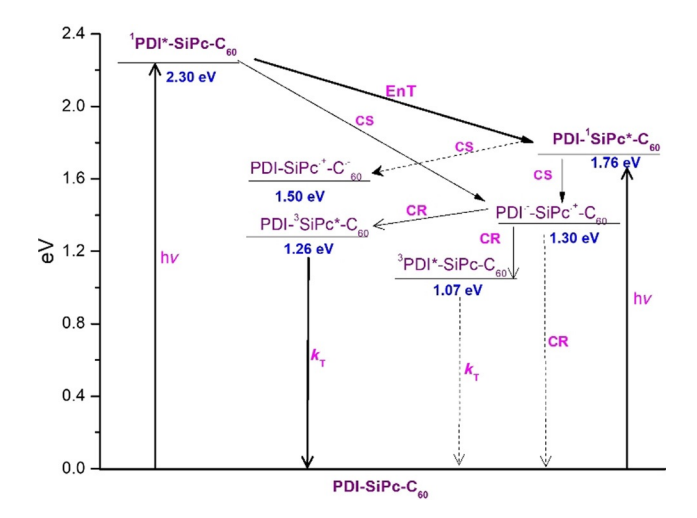


Figure 6. Energy level diagram depicting different photochemical events originating from $^{1}\text{PDI*}$ and $^{1}\text{SiPc*}$ in the PDI-SiPc-C₆₀ triad 1. Solid arrow—most likely process, dashed arrow—less likely process. EnT=energy transfer, CS=charge separation, CR=charge recombination, and T=triplet emission.

ning different time scales were systematically performed, and these findings are summarized below. An energy level diagram for the triad in toluene was also established as shown in Figure S5 (Supporting Information). Although energy and electron transfer events are thermodynamically feasible from ¹PDI*, electron transfer to PDI but not to C₆₀ from the ¹SiPc* could be realized in nonpolar toluene.

Transient pump-probe spectral studies

Transient absorption studies were performed on the dyad and triad in polar benzonitrile and nonpolar toluene. The compounds were excited at 698 nm, corresponding to SiPc excitation, and at 523 nm, corresponding to PDI excitation. Transient spectral feature of control compounds, SiPc and PDI are reported earlier (see Figure S6, Supporting Information).[19] In brief, ground state bleaching at 623 and 698 nm and peaks corresponding to singlet-singlet transitions at 477, 606, 651, 732, 847, 1390 and 1460 nm were observed in the case of SiPc. The 698 nm bleach peak also had contributions from stimulated emission. For PDI, ground state bleach at 486, 521, 561 and 593 nm and positive peaks at 634, 847 and 1000 nm, corresponding to excited state absorption, were observed. The 561 and 593 nm peaks also had contributions from stimulated emission. The decay and recovery of the positive and negative peaks tracked the lifetime of the individual probe being 5.1 ns for PDF and 5.7 ns for SiPc. Similar results were obtained for the spectra recorded in toluene.

In the present study, the photoprocesses of the dyad and triad were first investigated at the excitation wavelength of 523 nm, exciting selectively the PDI entity. The transient data was analyzed by generating decay associated spectra (DAS) of different photoproducts as a function of time. The obtained data was also compared with that obtained from monitoring the time profiles of the signature peaks in a multi-wavelength global analysis. Figure 7 and Figure S7 (Supporting Information) show the transient absorption spectra at the indicated delay times of the dyad and triad in benzonitrile and toluene, respectively.

In the case of the dyad PDI-SiPc, immediately after excitation of the PDI entity at 523 nm, the instantaneously formed ¹PDI*-SiPc revealed characteristic peaks originating from ¹PDI* (Figure 7a), which is a strong negative signal at 550 nm due to ground state bleach. Unlike in the case of PDI control, in which the recovery of this peak was slow, faster recovery of this peak was witnessed in the case of the dyad, which was accompanied by peaks corresponding to ¹SiPc*, especially the negative signal in the 700 nm, corresponding to ground-state bleach and positive signal in the 1300-1500 nm range corresponding to excited state absorption of ¹SiPc*. These results provide direct proof for singlet-singlet energy transfer in the dyad. Compared to the transient features of ¹SiPc*, in which the recovery/decay of the negative/positive peaks were slow, such peaks in the case of the dyad revealed faster recovery, with the appearance a new set of peaks characteristic of SiPc^{*+} at 880 nm and that of PDI* at 1010 nm, which provides direct proofs of photoinduced electron transfer from PDI-1SiPc* state



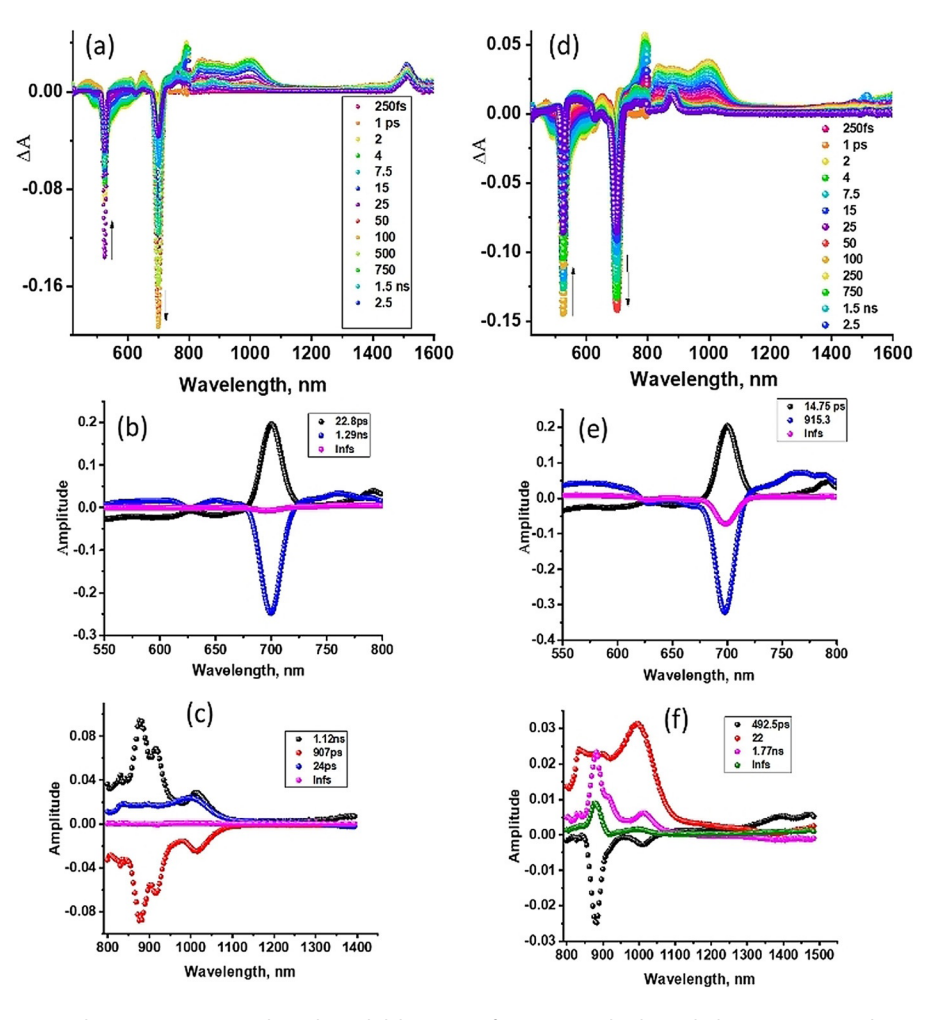


Figure 7. Femtosecond transient absorption spectra at the indicated delay times of (a) PDI-SiPc dyad 3 and (d) PDI-SiPc- C_{60} triad 1 in Ar-saturated benzonitrile, at the excitation wavelength of 523 nm exciting PDI entity selectively. The decay associated spectra for the visible and near-IR regions for dyad 3 (b and c) and triad 1 (e and f) are also shown.

to PDI*--SiPc*+ charge separated state (see Figure 7a at latter delay times).

In order to estimate the time constants for singlet-singlet energy transfer, decay associated spectra were generated, as shown in Figure 7 b. A positive peak at 700 nm characteristic of ¹SiPc* was observed at a time constant of 22.8 ps, suggesting that the energy transfer occurs at this time scale in the dyad.[32] A second negative component at 1.29 ns, much faster than the lifetime of control SiPc, suggested its involvement in additional electron transfer reaction. A third component with infinite time constant (> 3 ns) was also observed. In the near-IR region of 800-1400 nm, the decay associated spectra revealed four components (Figure 7c), the first one at 24 ps close to the 22.8 ps recorded for the ¹SiPc* formation. The second component with negative signals with a time constant of 907 ps was observed. From the location of peaks it could easily be ascribed to the formation of PDI*--SiPc*+ charge separated state. The third component with a mirror image of earlier negative signals at 1.12 ns was ascribed to the charge recombination process. Similar observations were also made in toluene (see Figure S7 a-c, Supporting Information). In this case, the time constants for energy transfer was 19.1 ps, whereas for charge separation and recombination, these values were 266 ps and >3 ns. By using these time constants and lifetime of control probes, energy transfer rate constant, $k_{\rm ENT}$ were calculated and were found to be $4.4\times10^{10}~{\rm s}^{-1}$ in benzonitrile and $5.2\times10^{10}~{\rm s}^{-1}$ in toluene, respectively. These values were about twice as much as that reported earlier for the PDI-SiPc dyad^[19] with longer donor–acceptor distance. Such a trend was also observed for the rate constants of charge separation. The calculated $k_{\rm CS}$ from the time constants were found to be $1.1\times10^9~{\rm s}^{-1}$ in benzonitrile and $3.8\times10^9~{\rm s}^{-1}$ in toluene, both nearly an order of magnitude higher due to spatial proximity compared to earlier reported PDI-SiPc dyad. That is, faster energy and charge transfer events in the present PDI-SiPc dyad was possible to witness.

The transient spectra for the PDI-SiPc- C_{60} triad at the excitation wavelength of 523 nm in benzonitrile is shown in Figure 7 d. Largely, the photochemical events tracked to those observed for the dyad. That is, singlet–singlet energy transfer to populate the ¹SiPc* state in the earlier time scales, and additional photochemical events from the ¹SiPc* state at the latter time scales to produce the charge separated state involving the energetically more accessible PDI, and not C_{60} , was wit-



nessed. This result was in contradiction to the earlier reported triad, 10, in which the spatially far PDI and spatially close C_{60} were both involved in the electron-transfer process. ^[19] On the contrary, in the present system, due to close proximity and facile reduction potential, PDI was the primary beneficiary in the electron process.

The time constants evaluated from the decay associated spectra (Figure 7 e,f) were found to be 14.8 ps for energy transfer, and 492.5 ps for charge separation processes. These values resulted in k_{ENT} and k_{CS} values of $6.7 \times 10^{10} \, \text{s}^{-1}$ and $2.0 \times 10^9 \, \text{s}^{-1}$, respectively, and were slightly higher than that obtained for the dyad and were also higher compared to the earlier reported triad. [19] The presence of a second electron acceptor, C₆₀, at the opposite end in the triad seems to accelerate both energy and charge separation processes in the triad. Such a trend was also observed for the triad in nonpolar toluene (Figure S7 d-f, Supporting Information). The time constants, from the decay associated spectra were found to be 12.45 ps for energy transfer, and 532 ps for charge separation processes were witnessed. These values resulted in $k_{\rm ENT}$ and $k_{\rm CS}$ values of 8.0 \times $10^{10} \, \text{s}^{-1}$ and $1.89 \times 10^9 \, \text{s}^{-1}$, respectively, once again, slightly higher than that reported for the previously described triad

Finally, transient spectra of the dyad and triad were recorded at the excitation wavelength of 689 nm, exciting selectively the SiPc entity. Figure 8 shows the results obtained for the dyad and triad in benzonitrile, whereas those for the measurements performed in toluene are shown in Figure S8 in the Supporting Information. In the case of both dyad and triad, the instantaneously formed ¹SiPc* revealed faster recovery/decay of the ¹SiPc* originated peaks and with appearance of new peaks corresponding to PDI*-SiPc*+ charge separated state in the

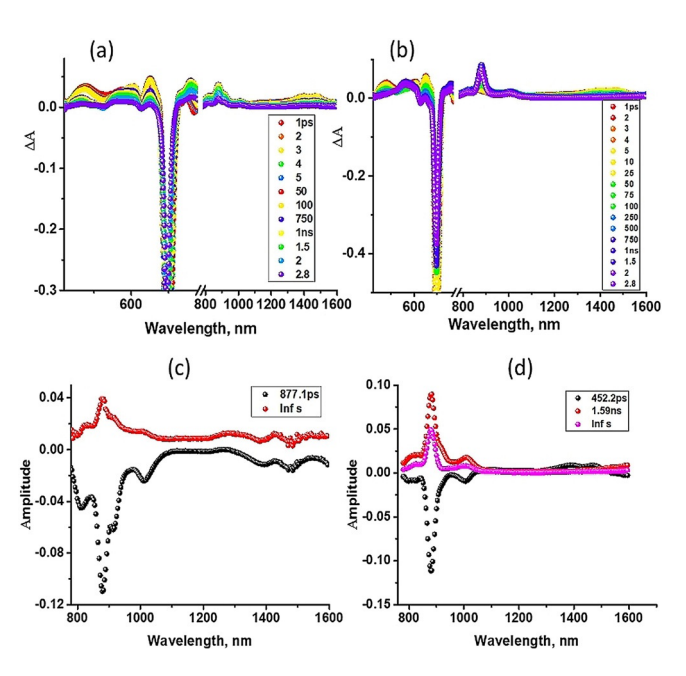


Figure 8. Femtosecond transient absorption spectra at the indicated delay times of (a) PDI-SiPc dyad **3** and (d) PDI-SiPc- C_{60} triad **1** in Ar-saturated benzonitrile, at the excitation wavelength of 689 nm exciting SiPc entity selectively. The decay associated spectra for the near-IR region are also shown.

case of the dyad and PDI*-SiPc*+- C_{60} charge separated state in the case of the triad. No evidence for formation of PDI-SiPc*+- C_{60} *- was observed indicating the electron transfer only involves the PDI entity and not C_{60} , as predicted from the energy level diagram in Figure S5 (Supporting Information). Selective charge separation in the presence of multiple electron acceptors has been possible to achieve in the present model compound.

Decay associated spectra were generated to identify the charge separation products and their kinetic information, and they are shown below each transient spectra in Figure 8 and Figure S8 (Supporting Information). In all cases, the spectral features characteristic of PDI*-SiPc*+ were clear. The time constants for the charge separation in benzonitrile for the dyad and triad were found to be 877 and 452 ps, respectively, which resulted in k_{CS} values of $1.1 \times 10^9 \text{ s}^{-1}$ and $2.2 \times 10^9 \text{ s}^{-1}$. Similarly, in toluene the time constants were found to be 523 and 582 ps, respectively, which resulted in k_{CS} values of $1.9 \times 10^9 \text{ s}^{-1}$ and $1.7 \times 10^9 \text{ s}^{-1}$. In all the cases the rate constants were an order of magnitude higher than that reported earlier for triad $9^{[19]}$, mainly due to decreased distance between SiPc and PDI.

A summary of energy and electron transfer rate constants for the present dyad and triad and those of the earlier reported ones are given in Table 2. As pointed earlier, both energy and electron transfer rates are higher for the present series of compounds due mainly "close" distance between the PDI and SiPc, especially the electron transfer rate constants, which are an order of magnitude higher. Positioning the PDI closer to SiPc also affected overall photochemical events in the triad, that is, no evidence of C₆₀ involvement in the charge separation process was witnessed. Generally, presence of C₆₀ accelerated the energy and electron transfer processes to some extent, perhaps due to subtle structural and electronic changes. In most of the cases, the charge separated state lasted over 3 ns, monitoring time window of our instrumental setup. Nanosecond transient spectra were also recorded to seek long-lived charge separated states. In all the cases strong signal characteristic of ³SiPc* was observed (Figure S9, Supporting Information). These results suggest the final lifetime of the charge separated state to be less than 20 ns (lower detection limit of our nanosecond transient spectrometer).

Table 2. Energy and charge separation rate constants for the PDI-SiPc dyad and PDI-SiPc- C_{60} triad series at the PDI and SiPc excitation wavelengths (see Figure 1 and Scheme 1 for structures). t.w. = this work.

Compound	Solvent	$k_{\rm ENT}$ [s ⁻¹]	$k_{\rm CS} [{\rm s}^{-1}]^{[{\rm a}]}$	$k_{\rm CS} [{\rm s}^{-1}]^{\rm [b]}$	Ref
PDI-SiPc, 3	PhCN	4.4×10 ¹⁰	1.1×10 ⁹	1.4×10 ⁹	t.w.
	toluene	5.2×10^{10}	3.8×10^{9}	1.9×10^{9}	t.w.
PDI-SiPc-C ₆₀ , 1	PhCN	6.7×10^{10}	2.0×10^{9}	2.2×10^{9}	t.w.
	toluene	8.0×10^{10}	1.9×10^{9}	1.7×10^{9}	t.w.
PDI-SiPc, 9	PhCN	2.6×10^{10}	2.52×10^{8}	-	[19]
	toluene	2.7×10^{10}	1.26×10^{8}	-	[19]
PDI-SiPc-C ₆₀ , 10	PhCN	2.9×10^{10}	8.25×10^{8}	-	[19]
	toluene	5.0×10^{10}	4.62×10^{8}		[19]

[a] At PDI excitation wavelength (523 nm). [b] At SiPc excitation (698 nm).



Conclusions

In summary, the present investigation highlights the importance of intramolecular distance between donor-acceptor entities in multimodular conjugates in governing the excited state energy and electron transfer events. Although in the case of the PDI-SiPc dyads, 3 and 9, the singlet-singlet excitation transfer followed by electron transfer leading to PDI*--SiPc*+ charge separated state was evident; the closer separation in the case of 3 made these photochemical events faster. Interestingly, in the case of triads, 1 and 10, the presence of C_{60} at the opposite side of PDI of SiPc, had few noticeable effects. First, both energy and charge transfer processes were slightly faster compared to the corresponding dyad. Second, involvement of C₆₀ in electron transfer was seldom seen in the case of 1 irrespective of whether (i) PDI or SiPc was excited, or (ii) changing solvent from polar to nonpolar. This was unlike for 10, for which charge separation competitively occurred involving both PDI and C₆₀ electron acceptors in both polar and nonpolar solvents upon PDI excitation. Further studies along these lines are in progress in our laboratories.

Experimental Section

Chemicals

All reagents used for synthesis and spectroscopic studies were analytical grade and are used as received.

Spectral, electrochemical and photophysical measurements

NMR spectra were acquired on a Bruker AC 300 spectrometer. Multiplicities are given as s (singlet), d (doublet), t (triplet), q (quartet), dd (doublet of doublets), and m (multiplet), and the coupling constants, *J*, are given in Hz. UV/Vis spectra were recorded either on a Helios Gamma spectrophotometer or a Shimadzu Model 2550 double-monochromator. Fluorescence spectra were recorded either on a PerkinElmer LS 55 luminescence spectrometer or Horiba Yvon Nanolog coupled with time-correlated single-photon counting with nanoLED excitation sources. A right angle detection method was used to record fluorescence emission. Matrix-assisted laser desorption/ionization time-of-flight (MALDI-TOF) mass spectra were obtained on a Bruker Microflex spectrometer.

Femtosecond transient absorption spectroscopy experiments were performed by using an ultrafast femtosecond laser source (Libra) by Coherent incorporating a diode-pumped, modelocked Ti:sapphire laser (Vitesse) and a diode-pumped intracavity doubled Nd:YLF laser (Evolution) to generate a compressed laser output of 1.45 W. For optical detection, a Helios transient absorption spectrometer coupled with a femtosecond harmonics generator, both provided by Ultrafast Systems LLC, was used. The sources for the pump and probe pulses were derived from the fundamental output of Libra (Compressed output 1.45 W, pulse width 100 fs) at a repetition rate of 1 kHz; 95% of the fundamental output of the laser was introduced into a TOPAS-Prime-OPA system with a 290-2600 nm tuning range from Altos Photonics Inc., (Bozeman, MT), while the rest of the output was used for generation of a whitelight continuum. Kinetic traces at appropriate wavelengths were assembled from the time-resolved spectral data. Data analysis was performed by using Surface Xplorer software supplied by Ultrafast Systems. All measurements were conducted in degassed solutions at 298 K. The estimated error in the reported rate constants is $\pm\,10\,\%.$

The nanosecond transient absorption measurement was done by using laser flash photolysis instrumental setup composed of a Opolette HE 355 LD pumped by a high-energy Nd:YAG laser with second and third harmonics OPO (tuning range 410–2200 nm, pulse repetition rate 20 Hz, pulse length 7 ns) with laser powers of 1.0–3 mJ pulse⁻¹. For spectral measurements, a Proteus UV-vis-NIR flash photolysis spectrometer (Ultrafast Systems, Sarasota, FL) with a fiberoptic delivered white light as probe and either a fast rise Si photodiode detector (covering 200–1000 nm range) or a InGaAs photodiode detector (covering 900–1600 nm range) was used. The output from the photodiodes and a photomultiplier tube was recorded using a digitizing Tektronix oscilloscope. Data analysis was performed using Surface Xplorer software from Ultrafast Systems.

Synthesis and characterization of compounds

PDI-CO₂H **2**,^[22] SiPc ref. **6**,^[20] PDI ref. **7**^[33] and C₆₀ ref. **8**^[20] were prepared as previously described. Column chromatography was performed on SiO₂ (40–63 mm) or using a Combiflash $^{\circ}$ $R_{\rm f}$ chromatography system (Teledyne Technologies, Inc., Thousand Oaks, CA).

PDI-SiPc-CHO 3: (tBu)₄SiPcCl₂ (30 mg, 0.04 mmol), 4-formylbenzoic acid (5.4 mg, 0.04 mmol), PDI-CO₂H 2 (29 mg, 0.04 mmol), and 1butyl-3-methylimidazolium bromide (BMIB, 1 drop) were mixed in 2-methoxyethyl ether (diglyme, 1 mL) in a 10 mL microwave reaction tube, which was then capped. The contents were stirred and microwave-irradiated to a set temperature of $180\,^{\circ}\text{C}$ for 30 min. The crude reaction mixture was poured into 0.5 m aqueous HCl and, the precipitate formed, collected by vacuum filtration. The resulting brown-green powder was dissolved in CH₂Cl₂ (100 mL). Filtration and removal of the solvent in vacuo provided the corresponding crude product, which was purified twice by a Combi-Flash® chromatographic method, by using normal-phase silica columns, firstly with CH2Cl2 and CH2Cl2/AcOEt mixture as eluants and followed by hexane and hexane/AcOEt mixture. 3.6 mg of PDI-SiPc-CHO 3 were obtained as a brown-green powder (6% yield). $^{1}\text{H NMR}$ (300 MHz, CDCl $_{3}$ 25 °C): δ 9.82–9.57 (8 H, m, H-Pc), 9.40 (1 H, s, CHO), 9.67 (1 H, s, H-PDI), 8.47 (4 H, d, J=8.1 Hz, H-Pc), 8.40 (2 H, s, H-PDI), 7,50 (1 H, t, J=7.7 Hz, H-Ar), 7.33 (2 H, d, J=7.7 Hz, H-Ar), 6.77 (2 H, d, J=8.2 Hz, H-Ar), 6.20 (2 H, d, J=8.4 Hz, H-Ar), 5,38 (2 H, d, J = 8.4 Hz, H-Ar), 5.32 (2 H, d, J = 8.2 Hz, H-Ar), 2.67 (2 H, m, 2x H₃C-<u>CH</u>-CH₃), 1,87-1,78 (36 H, m, 4xtBut), 1.18-1.09 (12 H, m, 12xCH $_{\rm 3)}$ ppm. UV/Vis (CHCl $_{\rm 3})~\lambda_{\rm max}~{\rm nm}^{-1}$ (log ε): 360 (4.92), 488 (4.48), 521 (4.63), 625 (4.58), 664 (4.52), 695 (5.38). HR-EM (MALDI-TOF, dithranol): m/z for $[C_{99}H_{78}Cl_4N_{10}O_9Si]^+$ calcd 1718.4484; found 1718.4670.

PDI-SiPc-C₆₀ 1: A mixture of C₆₀ (33 mg, 0.05 mmol), sarcosine (14 mg, 0.2 mmol), and PDi-SiPc-CHO **3** (25 mg, 0.01 mmol) in *o*-dichlorobenzene (3 mL) was stirred at 150 °C under argon atmosphere for 1 h. After cooling, the reaction mixture was purified by column chromatography (SiO₂; toluene →toluene/AcOEt 50:1, v/v) yielding 27 mg (75%) of PDI-SiPc-C₆₀ **1** as a brown solid. ¹H NMR (300 MHz, CDCl₃ 25 °C): δ 9.85–9.55 (8 H, m, H-Pc), 8.67 (2 H, s, H-PDI), 8.45 (4 H, d, J=8.0 Hz, H-Pc), 8.39 (2 H, s, H-PDI), 7.50 (1 H, t, J=7.7 Hz, H-Ar-PDI), 7.33 (2 H, d, J=7.7 Hz, H-Ar-PDI), 6,70 (2 H, br s, H-Ar-C₆₀), 6.19 (2 H, d, J=8.5 Hz, H-Ar-PDI), 5,35 (2 H, d, J=8.5 Hz, H-Ar-PDI), 5.26 (2 H, d, J=7.6 Hz, H-Ar-C₆₀), 4.63 (1 H, d, J=9.5 Hz, H-pyrrolidine), 4.28 (1 H, s, H-pyrrolidine), 3.87 (1 H, d, J=9.5 Hz, H-pyrrolidine), 2.67 (2 H, m, 2× H₃C-<u>CH</u>-CH₃), 2.20 (3 H, s, N-C<u>H₂</u>), 1.90–1.75 (36 H, m, 4×tBut), 1.19–1.09 (12 H, m, 12×CH₃₎ ppm. UV/Vis (CHCl₃) λ_{max} nm⁻¹ (log ε): 360 (4.96), 487 (4.47), 521 (4.63), 625



(4.53), 664 (4.47), 695 (5.34). HR-EM (MALDI-TOF, dithranol): m/z for $[C_{161}H_{83}Cl_4N_{11}O_8Si+H]^+$ calcd 2469.5094; found 2469.5107.

Acknowledgements

Á. Sastre Santos thanks the Ministerio de Economía, Industria *y* Competitividad of Spain and FEDER funds for the financial support (CTQ2017-87102-R). This work is funded by the National Science Foundation (Grant No. 1401188 to FD). The computational work was completed at the Holland Computing Center of the University of Nebraska, which receives support from the Nebraska Research Initiative.

Conflict of interest

The authors declare no conflict of interest.

Keywords: charge separation • energy transfer • fullerenes • perylene diimides • silicon phthalocyanines

- [1] K. Nikolaidou, S. Sarang, S. Ghosh, Nano Futur. 2019, 3, 012002.
- [2] P. K. Nayak, S. Mahesh, H. J. Snaith, D. Cahen, Nat. Rev. Mater. 2019, 4, 269–285.
- [3] A. Polman, M. Knight, E. C. Garnett, B. Ehrler, W. C. Sinke, Science 2016, 352, aad4424.
- [4] a) D. Gust, T. A. Moore, A. L. Moore, Acc. Chem. Res. 2009, 42, 1890–1898; b) D. Gust, T. A. Moore, A. L. Moore, Faraday Discuss. 2012, 155, 9–26; c) E. M. Pérez, N. Martín, Chem. Soc. Rev. 2008, 37, 1512–1519; d) K. Dirian, M. A. Herranz, G. Katsukis, J. Malig, L. Rodríguez-Pérez, D. Romero-Nieto, V. Strauss, N. Martín, D. M. Guldi, Chem. Sci. 2013, 4, 4335–4353; e) J. S. Lindsey, D. F. Bocian, Acc. Chem. Res. 2011, 44, 638–650; f) Y. Wang, H. Suzuki, J. Xie, O. Tomita, D. J. Martin, M. Higashi, D. Kong, R. Abe, J. Tang, Chem. Rev. 2018, 118, 5201–5241.
- [5] a) D. M. Guldi, A. Rahman, V. Sgobba, C. Ehli, Chem. Soc. Rev. 2006, 35, 471 – 487; b) J. N. Clifford, G. Accorsi, F. Cardinali, J. F. Nierengarten, N. Armaroli, C. R. Chemie 2006, 9, 1005-1013; c) N. Martín, L. Sánchez, M. A. Herranz, B. Illescas, D. M. Guldi, Acc. Chem. Res. 2007, 40, 1015 -1024; d) G. Bottari, G. de la Torre, D. M. Guldi, T. Torres, Chem. Rev. 2010, 110, 6768-6816; e) D. M. Guldi, V. Sgobba, Chem. Commun. 2011, 47, 606-610; f) D. González-Rodríguez, E. Carbonell, D. M. Guldi, Angew. Chem. Int. Ed. 2009, 48, 8032-8036; Angew. Chem. 2009, 121, 8176-8180; g) S. Fukuzumi, Phys. Chem. Chem. Phys. 2008, 10, 2283-2297; h) S. Fukuzumi, T. Kojima, J. Mater. Chem. 2008, 18, 1427 - 1439; i) S. Fukuzumi, T. Honda, K. Ohkubo, T. Kojima, Dalton Trans. 2009, 3880 -3889; j) S. Fukuzumi, K. Ohkubo, J. Mater. Chem. 2012, 22, 4575-4587; k) S. Fukuzumi, K. Ohkubo, T. Suenobu, Acc. Chem. Res. 2014, 47, 1455 -1464; I) M. E. El-Khouly, O. Ito, P. M. Smith, F. D'Souza, J. Photochem. Photobiol. C 2004, 5, 79 - 104; m) F. D'Souza, O. Ito, Coord. Chem. Rev. 2005, 249, 1410-1422; n) F. D'Souza, O. Ito, Chem. Commun. 2009, 4913-4928; o) F. D'Souza, A. S. D. Sandanayak, O. Ito, J. Phys. Chem. Lett. 2010, 1, 2586-2593; p) F. D'Souza, O. Ito, Chem. Soc. Rev. 2012, 41, 86-96; q) F. D'Souza, O. Ito, In Multiporphyrin Array: Fundamentals and Applications (Ed.: D. Kim), Pan Stanford Publishing, Singapore, 2012, Chapter 8, pp. 389-437; r) C. B. Kc, F. D'Souza, Coord. Chem. Rev. 2016, 322, 104-141; s) X. Ji, J. Wang, L. Mei, W. Tao, A. Barrett, Z. Su, S. Wang, G. Ma, J. Shi, S. Zhang, Adv. Funct. Mater. 2018, 28, 1870061.
- [6] a) J. L. Sessler, C. M. Lawrence, J. Jayawickramarajah, Chem. Soc. Rev. 2007, 36, 314–325; b) S. Fukuzumi, K. Ohkubo, F. D'Souza, J. L. Sessler, Chem. Commun. 2012, 48, 9801–9815; c) G. Ulrich, R. Ziessel, A. Harriman, Angew. Chem. Int. Ed. 2008, 47, 1184–1201; Angew. Chem. 2008, 120, 1202–1219; d) M. El-Khouly, S. Fukuzumi, F. D'Souza, ChemPhys-Chem 2014, 15, 30–47; e) N. Armaroli, V. Balzani, Angew. Chem. Int. Ed. 2007, 46, 52–66; f) V. Balzani, A. Credi, M. Venturi, ChemSusChem 2008,

- 1, 26–58; g) S. Ye, C. Ding, R. Chen, F. Fan, P. Fu, H. Yin, X. Wang, Z. Wang, P. Du, C. Li, *J. Am. Chem. Soc.* **2018**, *140*, 3250–3256.
- [7] a) H. Imahori, T. Umeyama, S. Ito, Acc. Chem. Res. 2009, 42, 1809-1818; b) T. Umeyama, H. Imahori, Energy Environ. Sci. 2008, 1, 120-133; c) T. Hasobe, Phys. Chem. Chem. Phys. 2010, 12, 44-57; d) N. S. Lewis, D. G. Nocera, Proc. Natl. Acad. Sci. USA 2006, 103, 15729-15735; e) D. G. Nocera, Inorg. Chem. 2009, 48, 10001-10017; f) P. V. Kamat, J. Phys. Chem. C 2007, 111, 2834-2860; g) E. Schwartz, S. Le Gac, J. J. L. M. Cornelissen, R. J. M. Nolte, A. E. Rowan, Chem. Soc. Rev. 2010, 39, 1576-1599; h) P. Erwin, S. M. Conron, J. H. Golden, K. Allen, M. E. Thompson, Chem. Mater. 2015, 27, 5386-5392; i) Y. Nakamura, N. Aratani, A. Osuka, Chem. Soc. Rev. 2007, 36, 831-845; j) T. Kamimura, K. Ohkubo, Y. Kawashima, S. Ozako, K. Sakaguchi, S. Fukuzumi, F. Tani, J. Phys. Chem. C 2015, 119, 25634-25650; k) V. M. Blas-Ferrando, J. Ortiz, K. Ohkubo, S. Fukuzumi, F. Fernández-Lázaro, Á. Sastre-Santos, Chem. Sci. 2014, 5, 4785-4793; I) M. Sekita, B. Ballesteros, F. Diederich, D. M. Guldi, G. Bottari, T. Torres, Angew. Chem. Int. Ed. 2016, 55, 5560-5564; Angew. Chem. 2016, 128, 5650-5654; m) M. R. Wasielewski, Acc. Chem. Res. 2009, 42, 1910-1921; n) Y. Wu, R. M. Young, M. Frasconi, S. T. Schneebeli, P. Spenst, D. M. Gardner, K. E. Brown, F. Würthner, J. F. Stoddart, M. R. Wasielewski, J. Am. Chem. Soc. 2015, 137, 13236-13239; o) D. R. Whang, D. H. Apaydin, ChemPhotoChem 2018, 2, 148 – 160.
- [8] a) P. E. Hartnett, S. M. Dyar, E. A. Margulies, L. E. Shoer, A. W. Cook, S. W. Eaton, T. J. Marks, M. R. Wasielewski, Chem. Sci. 2015, 6, 402–411; b) L. Martín-Gomis, K. Ohkubo, F. Fernández-Lázaro, S. Fukuzumi, Á. Sastre-Santos, Chem. Commun. 2010, 46, 3944–3946; c) L. Martín-Gomis, G. Rotas, K. Ohkubo, F. Fernández-Lázaro, S. Fukuzumi, N. Tagmatarchis, Á. Sastre-Santos, Nanoscale 2015, 7, 7437–7444; d) S. Pla, M. Niemi, L. Martín-Gomis, F. Fernández-Lázaro, H. Lemmetyinen, N. V. Tkachenko, Á. Sastre-Santos, Phys. Chem. Chem. Phys. 2016, 18, 3598–3605; e) M. Wang, W. Zhan, Acc. Chem. Res. 2016, 49, 2551–2559.
- [9] D. M. Stoltzfus, J. E. Donaghey, A. Armin, P. E. Shaw, P. L. Burn, P. Meredith, Chem. Rev. 2016, 116, 12920 – 12955.
- [10] F. D'Souza, O. Ito, Sci. Prog. 2013, 96, 369-397.
- [11] H. Langhals, Heterocycles 1995, 40, 477.
- [12] Z. Zhang, J. Yuan, Q. Wei, Y. Zou, Front. Chem. 2018, 6, 414.
- [13] A. Nowak-Król, K. Shoyama, M. Stolte, F. Würthner, Chem. Commun. 2018, 54, 13763 – 13772.
- [14] G. de la Torre, G. Bottari, T. Torres, Adv. Energy Mater. 2017, 7, 1601700.
- [15] N. R. R. S. Gobo, T. J. Brocksom, K. T. de Oliveira, Curr. Org. Synth. 2017, 15, 1132 – 1155.
- [16] M.-E. Ragoussi, T. Torres, *Chem. Asian J.* **2014**, *9*, 2676–2707.
- [17] N. Martín, L. Sánchez, B. Illescas, I. Pérez, Chem. Rev. 1998, 98, 2527 2548.
- [18] A. Hirsch, Phys. Status Solidi 2006, 243, 3209-3212.
- [19] L. Martín-Gomis, F. Peralta-Ruiz, M. B. Thomas, F. Fernández-Lázaro, F. D'Souza, Á. Sastre-Santos, Chem. Eur. J. 2017, 23, 3863 3874.
- [20] L. Martín-Gomis, K. Ohkubo, F. Fernández-Lázaro, S. Fukuzumi, A. Sastre-Santos, Org. Lett. 2007, 9, 3441 3444.
- [21] L. Martín-Gomis, K. Ohkubo, F. Fernández-Lázaro, S. Fukuzumi, Á. Sastre-Santos, J. Phys. Chem. C 2008, 112, 17694 17701.
- [22] F. J. Céspedes-Guirao, L. Martin-Gomis, K. Ohkubo, S. Fukuzumi, F. Fernández-Lázaro, Á. Sastre-Santos, Chem. Eur. J. 2011, 17, 9153–9163.
- [23] L. Martín-Gomis, E. M. Barea, F. Fernández-Lázaro, J. Bisquert, Á. Sastre-Santos, J. Porphyrins Phthalocyanines 2011, 15, 1004 1010.
- [24] L. M. Arellano, L. Martin-Gomis, H. B. Gobeze, M. Barrejon, D. Molina, M. J. Gomez-Escalonilla, J. L. G. Fierro, M. Zhang, M. Yudasaka, S. Iijima, F. D'Souza, F. Langa, Á. Sastre-Santos, J. Mater. Chem. C 2015, 3, 10215 – 10224.
- [25] G. Rotas, L. Martín-Gomis, K. Ohkubo, F. Fernández-Lázaro, S. Fukuzumi, N. Tagmatarchis, Á. Sastre-Santos, Chem. Eur. J. 2016, 22, 15137 – 15143.
- [26] M. Maggini, G. Scorrano, M. Prato, J. Am. Chem. Soc. 1993, 115, 9798–9799.
- [27] J. R. Lakowicz, Principles of Fluorescence Spectroscopy, 3rd ed., Springer, Singapore, 2006.
- [28] Gaussian 16, Revision A.03, M. J. Frisch, G. W. Trucks, H. B. Schlegel, G. E. Scuseria, M. A. Robb, J. R. Cheeseman, G. Scalmani, V. Barone, G. A. Petersson, H. Nakatsuji, X. Li, M. Caricato, A. V. Marenich, J. Bloino, B. G. Janesko, R. Gomperts, B. Mennucci, H. P. Hratchian, J. V. Ortiz, A. F. Izmaylov, J. L. Sonnenberg, D. Williams-Young, F. Ding, F. Lipparini, F. Egidi, J. Goings, B. Peng, A. Petrone, T. Henderson, D. Ranasinghe, V. G. Zakrzew-



ski, J. Gao, N. Rega, G. Zheng, W. Liang, M. Hada, M. Ehara, K. Toyota, R. Fukuda, J. Hasegawa, M. Ishida, T. Nakajima, Y. Honda, O. Kitao, H. Nakai, T. Vreven, K. Throssell, J. A. Montgomery, Jr., J. E. Peralta, F. Ogliaro, M. J. Bearpark, J. J. Heyd, E. N. Brothers, K. N. Kudin, V. N. Staroverov, T. A. Keith, R. Kobayashi, J. Normand, K. Raghavachari, A. P. Rendell, J. C. Burant, S. S. Iyengar, J. Tomasi, M. Cossi, J. M. Millam, M. Klene, C. Adamo, R. Cammi, J. W. Ochterski, R. L. Martin, K. Morokuma, O. Farkas, J. B. Foresman, D. J. Fox, Gaussian, Inc., Wallingford CT, **2016**.

- [29] GaussView, Version 6.0.16, Roy Dennington, Todd A. Keith, and John M. Millam, Semichem Inc., Shawnee Mission, KS, 2016.
- [30] a) D. Rehm, A. Weller, Isr. J. Chem. 1970, 8, 259–271; b) N. Mataga, H. Miyasaka, in *Electron Transfer*; (Eds. J. Jortner, M. Bixon), Wiley, New York, 1999, part 2, pp. 431–496.
- [31] The free energy change for charge separation (ΔG_{CS}) from the singlet excited state ¹SiPc* within the donor-acceptor system is calculated in benzonitrile by using spectroscopic, computational and electrochemical data following equations $-\Delta G_{\text{CR}} = E_{\text{ox}} E_{\text{red}} + \Delta G_{\text{S}}$ and $-\Delta G_{\text{CS}} = \Delta E_{00} (-\Delta G_{\text{CR}})$, in which ΔE_{00} and ΔG_{CS} correspond to the energy of excited singlet state and electrostatic energy, respectively. E_{ox} and E_{red} represent the oxidation potential of the electron donor (SiPc) and the reduction potential of the electron acceptors (PDI and C60), respectively. The term ΔG_{S} refers to the static Coulombic energy, calculated by using the "dielectric continuum model" according to the following equation.

$$\Delta G_{S} = e^{2} / 4\pi \varepsilon_{0} \left[\left(\frac{1}{2} R_{+} + \frac{1}{2} R_{-} \right) \Delta \left(\frac{1}{\varepsilon_{R}} \right) - \frac{1}{R_{CC} \varepsilon_{R}} \right]$$

Symbols ε_0 and ε_R represent vacuum permittivity and dielectric constant (26 and 2.38, respectively for benzonitrile and toluene) of the solvent used for photochemical and electrochemical studies, respectively. $R_{\rm CC}$ is the center-to-center distance between donor and acceptor entities (center-to-center distance between SiPc and PDI, and SiPc and C_{60} were 13.8 and 11.6 Å, respectively). The symbols R_+ and R_- (6.55 Å for SiPc, 5.2 Å for PDI and 3.6 Å computed structure) refer to radii of the cation and anion species, respectively.

- [32] C. B. Kc, K. Stranius, P. D'Souza, N. K. Subbaiyan, H. Lemmetyinen, N. K. Tkachenko, F. D'Souza, *J. Phys. Chem. C* **2013**, *117*, 763–773.
- [33] H.-A. Klok, J. R. Hernández, S. Becker, K. Müllen, J. Polym. Sci. Part A **2001**, *39*, 1572–1583.

Manuscript received: December 11, 2019 Accepted manuscript online: January 21, 2020 Version of record online: March 20, 2020